CRYSTAL GROWTH & DESIGN

pubs.acs.org/crystal

Article

Effect of Substituent Exchange on Optical Anisotropy in Multicomponent Isostructural Materials Containing Sulfathiazole and 2-Aminopyridine Derivatives

Joanna Wojnarska, Marlena Gryl,* Tomasz Seidler, and Katarzyna M. Stadnicka

Cite This: *Cryst. Growth Des.* 2020, 20, 6535−6544

Read Online

ACCESS | Metrics & More | Article Recommendations | Supporting Information

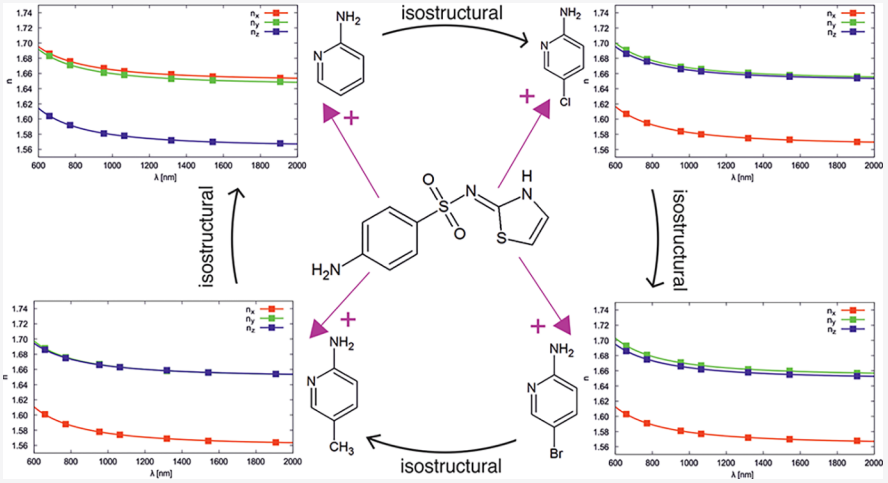

ABSTRACT: Four isostructural, multicomponent materials containing sulfathiazole and 2-aminopyridine substituted in the *para* position by H/CH_3/Cl/Br have been investigated. The crystal structures of these solids were determined using data from single-crystal X-ray diffraction measurements. The similarity of the crystal packing was studied using XPac and CrystalCMP programs as well as the packing similarity tool implemented in the Mercury software. The analysis of quantitative similarity parameters showed that the least similar geometrical arrangement is observed for H → Br interchange, while Cl → CH_3 exchange has the smallest influence on the molecular packing. These can be easily explained by the differences in the size and properties of the 2-aminopyridine substituent. Refractive indices of all materials were measured using the immersion oil method and calculated using the (Q)LFT approach. The observed variations in refractive indices were discussed in relation to the packing of the structural components and were correlated with the variations in polarizabilities of 2-aminopyridine derivatives.

1. INTRODUCTION

During the last few decades, material scientists have pursued the know-how in the rational design of crystalline functional materials. The implementation of the crystal engineering paradigm[1−3] brought scientists closer to achieving this goal. Predicting and controlling intermolecular interactions allowed a move from conventional synthetic routes[4−6] to cocrystallization, resulting in multicomponent functional solids.[7−9] In order to select proper molecules for a substantial physical effect to take place, it is crucial to understand the influence of two factors on the material properties. The first is the type of the building block and in particular its electronic properties. The second is the mutual orientation of molecules in a crystal structure (packing effect) along with the intermolecular interactions found between the molecules. The determination of the dominant factor for a particular property is crucial for engineering of materials with substantial physical effects. From an experimental point of view, we can solve this conundrum by looking at two phenomena: polymorphism and isostructurality. The first became a widely used playground for studies on structure−property relations[10,11] fueled by the developments of the pharmaceutical industry.[12] The second phenomenon can provide data on the structural origin of the material properties, mainly from the viewpoint of crystal components. Materials are classified as isostructural when they exhibit substantial

Received: May 29, 2020
Revised: September 4, 2020
Published: September 8, 2020

similarity of the molecular arrangement in a crystal structure, despite obvious differences in building block composition.[13] Multiple studies on solubility,[14,15] melting points,[16] and thermodynamic stability[17] in isostructural materials show that the resemblance in crystal architecture does not guarantee identical material properties. As isostructural materials have very similar crystal structures, the differences in properties are usually a result of dissimilarities in the crystal building blocks.[12] In most cases, crystal components differ by one substituent; therefore, isostructurality can be the source of information on the significance of that particular functional group/atom (i.e., its shape, size, and electronic properties) for the material properties.[12] Studies on isostructurality could be of particular interest for the controlled design of new optical materials, and in particular for crystalline materials with a high refractive index and substantial linear birefringence, so important in practical applications.[18,19] It is well-known that the magnitude of the refractive index is determined, among other factors, by the frequency-dependent molecular polarizability.[20] This relation is used in the Lorentz−Lorentz equation,[21,22] giving a valid approximation of refractive index determined e.g. for solutions. The situation in a crystal can be more complex due to optical anisotropy. The alterations of refractive indices with respect to crystal directions have been proven to be strongly influenced by the packing of molecules in the solid state.[23−26] The orientation of building blocks in a crystal structure is still difficult to predict, especially in dealing with multicomponent materials. From the viewpoint of materials design it would be ideal to find a perfect arrangement of the molecules in the solid state and tune the properties by selectively changing one or more substituents while retaining the original crystal packing. Unfortunately, isostructurality is less common than, for example, polymorphism. A small sensitivity of the molecular arrangement to the change in the substituent is required for an isostructural phenomenon to occur. For this reason the most often observed exchange is found to be the chloro−methyl transformation, as those substituents have similar shapes and sizes.[27,28] It is expected that isostructurality will be more common in multicomponent crystals, as the change of substituent in one component is less significant in comparison to an identical exchange in a single-component solid.[12] However, further research needs to be conducted in order to understand and quantify the changes of physical properties of the solid-state systems due to the small variations in functional groups of their components.

In this work, we present a series of isostructural, multicomponent materials containing a sulfathiazole molecule (STZ; 4-amino-*N*-(1,3-thiazol-2-yl)benzenesulfonamide) and 2-aminopyridine substituted in the *para* position by H/CH_3/Cl/Br. Sulfathiazole is an example of a sulfa drug showing antimicrobial properties.[29] There are known five polymorphs of STZ; some of them share similar 1D or 2D patterns,[30] and there are several sulfonamide derivatives which form isostructural crystals.[31−33] Until now, to the best of our knowledge, there have been no previous studies of isostructural multicomponent materials containing sulfonamide derivatives. The crystal structures of the isostructural solids discussed herein were determined experimentally using X-ray diffraction data and compared with each other using XPac[34] and CrystalCMP[35] software as well as a packing similarity tool from the Mercury program.[36] The refractive indices of all the materials were determined experimentally via the immersion oil method and were calculated using a (Q)LFT theoretical approach.[37−40] The observed differences in refractive indices of the studied materials were correlated with the packing of molecules in the crystal. The study of the structure−property relationship allowed for the analysis of the substituent influence on the optical anisotropy of sulfonamide-based isostructural materials.

2. EXPERIMENTAL SECTION

2.1. Cocrystallization. The studied materials were obtained using a slow evaporation technique. Sulfathiazole and 2-aminopyridine substituted in the *para* position by H/CH_3/Cl/Br were dissolved in methanol at room temperature and combined in a 1:1 molar ratio. The structural formulas of the substrates are presented in Figure S1. The cocrystallization experiment was conducted under ambient conditions and after several days, from four different solutions, the crystals of 2-aminopyridine sulfathiazole ⟨1/1⟩ (STZ2ap), 2-amino-5-methylopyridine sulfathiazole ⟨0.57^{+}:0.43/0.43:0.57^{-}⟩ (STZ2a5mp), 2-amino-5-chloropyridine sulfathiazole ⟨1/1⟩ (STZ2a5Clp), and 2-amino-5-bromopyridine sulfathiazole ⟨1/1⟩ (STZ2a5Brp) were obtained. The naming scheme was constructed from the nomenclature devised by some of us.[41] In the case of STZ2a5mp a 0.43:0.57 cocrystal to salt ratio was obtained. We have treated this as a nonstoichiometric case and adapted the nomenclature accordingly.

2.2. Single-Crystal X-ray Diffraction. Crystal structures of all the materials were determined using data collected from single-crystal X-ray diffraction experiments conducted at 25 °C using Mo Kα radiation. The measurements for STZ2ap, STZ2a5mp, and STZ2a5Clp were performed on a Rigaku XtaLAB Synergy S diffractometer and for STZ2a5Brp on a Rigaku SuperNova diffractometer. Data collection, cell refinement, and data reduction were carried out using CrysAlisPro (171.38.41r, 2015) or CrysAlisPro (1.171.40.14e, 2018).[42] The structures of STZ2ap, STZ2a5mp, and STZ2a5Clp were solved using direct methods in SHELXT2014,[43] and the structure of STZ2a5Brp was solved using SIR92.[44] The refinement of all crystal structures was conducted using a nonlinear least-squares method incorporated in SHELXL2018.[45] All H atoms bonded to N atoms were found in difference Fourier maps and refined with U_{iso} = 1.2U_{eq}(N). The H atoms connected to C atoms were located in geometrically calculated positions and refined using a riding model. Details on crystal data, intensity measurement conditions, and structure refinement are presented in Table S1. The resulting bond lengths, valence angles, and torsion angles for the structures are given in Table S2.

2.3. Theoretical Calculations. The theoretical electron density was obtained from periodic calculations using Crystal17[46,47] software at the B3LYP/POB-TZVP level of theory. During these calculations the positions of atoms were optimized while the unit cell parameters were kept fixed. The geometrical parameters for the optimized structures are given in Table S3. For STZ2a5mp two optimizations were performed due to observed disorder on H atoms (separately for co-crystal (set A) and salt (set B)). A topological analysis was carried out using the TOPOND program.[48,49] Calculations of refractive indices were carried out using a local field approach.[37−40] Molecular properties were calculated using Gaussian16[50] at the MP2/6-311++G(d,p) level with frequency dispersion included in static and dynamic polarizability tensors at the B3LYP level. The partitioning of the molecular (ionic) polarizabilities into the atomic contributions was performed with AIMAll.[51]

2.4. Measurements of Refractive Indices. The theoretically determined values of refractive indices were compared with experimental measurements carried out using a microscopic immersion oil method; details of such an experiment are described in the Supporting Information as well as in some of our earlier works.[26] As most of the examined crystals were needle-shaped, subsequent measurements of the linear birefringence using an Ehringhaus compensator were necessary to confirm the observed values of refractive indices. Additional difficulties in the measurements were encountered for STZ2ap and STZ2a5mp, where placement of

https://dx.doi.org/10.1021/acs.cgd.0c00743
Cryst. Growth Des. 2020, 20, 6535−6544

the crystals in some immersion oils caused slow but persistent recrystallization (see Figure S2).

3. RESULTS AND DISCUSSION

3.1. Crystal Structures. All of the studied crystalline materials follow the symmetry of the monoclinic space group $P2_1/n$ and have similar lattice parameters (Table S1). Each of the presented crystalline solids, except STZ2a5mp, is a co-crystal, and its asymmetric unit consists of one sulfathiazole molecule and one 2-aminopyridine molecule or one *para*-substituted 2-aminopyridine molecule (Figure S3a,c,d). In the case of STZ2a5mp, the H atom between sulfathiazole N8 and pyridine N2A atoms (Figure S3b) is disordered into two positions with occupancies of 0.43(3) and 0.57(3), respectively. The existence of salt and co-crystal products can be explained by comparing ΔpK_a values of the crystal building blocks, calculated as the difference between the pK_a values of a base and an acid. The obtained values are as follows: 2.53, 2.55, 0.38, and 0.02 for STZ2a5Clp, STZ2a5Brp, STZ2ap, and STZ2a5mp, respectively. Values between 0 and 3 are known to indicate the formation of a salt, a co-crystal, or both products.[52] The only flexible building block in the crystal structures is STZ. A comparison of STZ conformation among the analyzed structures shows that they are almost identical (see Figure 1 and Table 1). The maximum difference of ca. 5° observed for the torsion angle $S_1N_1C_7S_{11}$ and the changes in valence angles of up to 2° are negligible. Such a similarity in the conformation of STZ suggests that intermolecular interactions present in the crystal structures should form matching synthons and be comparable in strength.

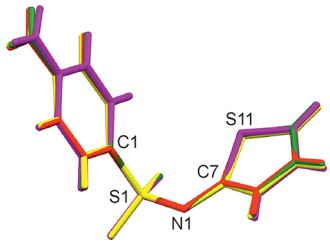

Figure 1. Superposition of STZ molecules from STZ2ap (magenta), STZ2a5mp (yellow), STZ2a5Clp (green), and STZ2a5Brp (red).

In each of the presented materials the strongest hydrogen bond is N8−H8···N2A, connecting the thiazole ring of STZ and the pyridine derivative (Table S4). This interaction together with a N1A−H1A1···N1 hydrogen bond forms the synthon $R_2^2(8)$, which is repeated in each of the studied crystal structures and which forms a building unit called here and referred to later as a building brick (Figure 2a). Building bricks are connected with each other by N−H···O type hydrogen bonds formed between the amino group of STZ and both oxygen atoms from the sulfonamide group: N4−H42···O1 ($1 + x, y, z$) and N4−H41···O2 ($1/2 + x, 1/2 - y, -1/2 + z$). In the structures one can also recognize a weak N1A−H1A2···N4 ($-1 + x, y, z$) interaction between the bricks (Table 3). In all materials the two weak contacts C6A−H6A···O1 ($-1/2 + x, 1/2 - y, -1/2 + z$) and C5A−H5A···O2 ($-1 + x, y, -1 + z$) are also observed. Furthermore, in STZ2a5Clp and STZ2a5Brp the halogen atom interacts weakly with the H3−C3 donor. These interactions lead to the formation of a layer with a thickness of ca. $0.75b$ expanding in the (010) plane (Figure 2b and Figure S4). The layers are repeated along [010] by inversion (Figure 2c). The relative orientation of layers is stabilized by the presence of weak, dispersive $\pi\cdots\pi$ and C−H···π interactions (Table S5 and Figure 3). The $\pi\cdots\pi$ contact between the thiazole rings of STZ is the strongest in STZ2ap (Cg···Cg = 3.584(1) Å, slippage 1.12 Å) and its strength decreases with an increasing size of the 2-aminopyridine substituent (for STZ2a5Brp: Cg···Cg = 3.839(1) Å, slippage 1.50 Å). An opposite behavior is observed for the $\pi\cdots\pi$ contact between the thiazole ring and 2-aminopyridine ring (Table S5). There are no significant changes in the strength of the C9−H9···Cg2 ($1 - x, 1 - y, 1 - z$) interaction (Cg2 is the centroid of the STZ six-membered aromatic ring) among all of the materials.

3.2. Isostructurality Analysis. The essential condition for the isostructurality of materials is the similarity of their unit cells.[54] For this reason, the unit-cell similarity index Π,[55] which compares lattice cell parameters, was calculated

$$\Pi = \frac{a + b + c}{a' + b' + c'} - 1$$

where a, b, c and a', b' c' are orthogonalized lattice parameters of their unit cells and $a + b + c > a' + b' + c'$. The unit cell parameters were transformed to an orthogonal unit cell using the Löwdin method as described by Fábián et al.[13] The Π parameters calculated against lattice parameters of STZ2ap are equal to 0.024, 0.022, and 0.044 for STZ2a5mp, STZ2a5Clp and 2a5Brp, respectively. Π values close to zero prove that the materials have similar unit cells and can be isostructural. Additionally, on the basis of the calculated values, the best resemblance among the four studied crystal structures is expected between STZ2a5mp and STZ2a5Clp, which is not surprising, as the chlorine atom and methyl group have similar sizes and shapes.[27]

The packing of molecules in the crystal was compared using the software XPac.[32] In the XPac approach the analysis of two crystal structures is based on computing the mean differences in all intermolecular angles (δ_a) and planes (δ_p) of molecular clusters representing the whole structures. The cluster contains one central molecule and its neighboring molecules (typically 14). Depending on the number of matches between clusters, similarity in 0D/1D/2D/3D dimensions can be acquired. The qualitative parameters of isostructurality x and d, derived from δ_a and δ_p, can be calculated.[32] The dissimilarity index x describes how much two structures differ from perfect geometrical similarity, and the parameter d gives a measure

Table 1. Selected Torsion and Valence Angles in STZ Molecules (Values in deg)

	$C_1S_1N_1C_7$	$S_1N_1C_7S_{11}$	$C_1S_1N_1$	$S_1N_1C_7$	$N_1C_7S_{11}$
STZ2ap	−80.4(1)	−2.1(2)	107.4(1)	120.7(1)	129.7(1)
STZ2a5mp	−79.9(1)	−7.5(2)	108.1(1)	121.6(1)	128.2(2)
STZ2a5Clp	−80.0(2)	−5.9(2)	106.9(1)	120.3(1)	129.7(1)
STZ2a5Brp	−79.8(2)	−7.1(2)	106.8(1)	119.9(1)	129.9(2)

https://dx.doi.org/10.1021/acs.cgd.0c00743
Cryst. Growth Des. 2020, 20, 6535−6544

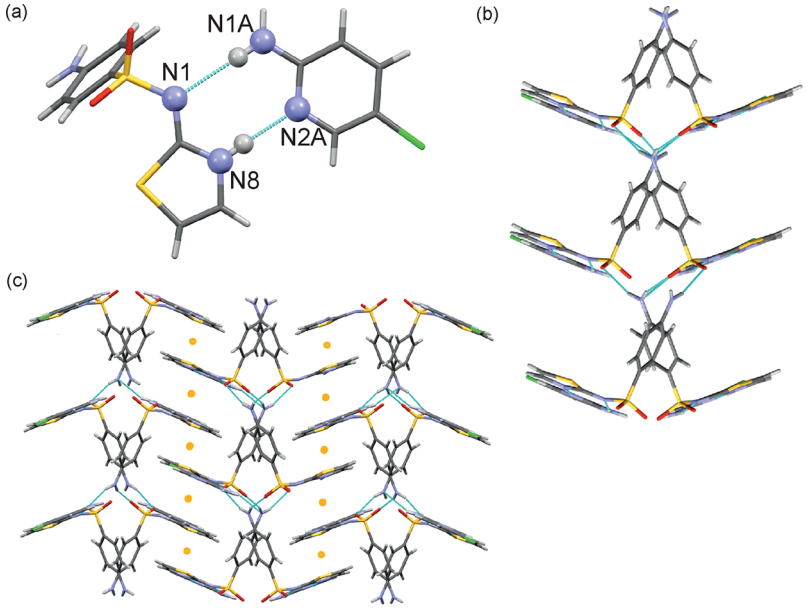

Figure 2. Basic building unit, i.e. building brick stabilized by formation of synthon $R_2^2(8)$ (a), side view (along [101]) of a layer extended in the (010) plane (b), and relation of the layers with inversion centers marked as yellow dots (c). The figures were prepared for STZ2a5Clp. A similar arrangement is observed in the remaining isostructural materials.

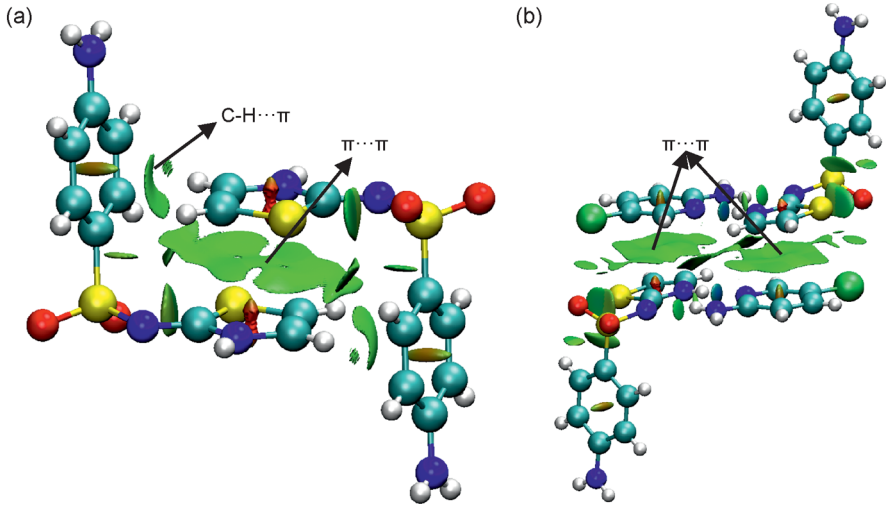

Figure 3. NCI regions showing a C9−H9···Cg2 $(1 - x, 1 - y, 1 - z)$ interaction and $\pi\cdots\pi$ contacts between the thiazole rings of STZ (a) and $\pi\cdots\pi$ interactions formed between the thiazole ring and 2-aminopyridine ring (b). The irregular green surfaces indicate the presence of weak dispersive interactions.[53] The figures were prepared for STZ2a5Clp. The wave functions for the calculation of the NCI index were obtained using Gaussian16 software[50] at the M052X/6-311+G(2df,2p) level of theory.

of the differences in intermolecular distances between clusters. Application of the XPac program, with STZ as the central molecule of the cluster, showed that each two pairs of crystal structures exhibit 3D similarity. The calculated qualitative parameters describing isostructurality (Table 2) indicate that the most similar geometrical arrangement of molecules is observed between STZ2a5mp and STZ2a5Clp. As mentioned before, this is not surprising due to the commonly known chloro−methyl exchange. The largest x and d parameters, indicating the smallest packing similarity, are observed for H → Br interchange, which is understandable due to the differences in size and electronic properties of these two substituents. a better resemblance of molecular arrangement is displayed by Br → Cl/CH_3 exchange in comparison to H → Cl/CH_3 exchange, which is consistent with the variation of the size of substituent. Identical conclusions were gathered from a molecular arrangement comparison performed using CrystalCMP[35] and the packing similarity tool from the Mercury program[36] (for details see the Supporting Information).

3.3. Intermolecular Interactions. Intermolecular interactions were studied through topological analysis of the theoretical electron density to examine the influence of the 2-aminopyridine substituent on the crystal packing. The topological descriptors of selected hydrogen bonds and other weak interactions are given in Table 3. In all materials the strongest hydrogen bond is N8−H8···N2A with an intermediate character between closed shell and shared shell $(E(r)/\rho(r) < 0)$. This interaction, together with N1A−H1A···N1, is responsible for the formation of the building brick unit. There are no significant differences in energies of N8−H8···N2A and

https://dx.doi.org/10.1021/acs.cgd.0c00743
Cryst. Growth Des. 2020, 20, 6535−6544

Table 2. Dissimilarity Indices x (Bottom Left Triangular Section of Matrix) and Distance Parameters $d \times 10^{-2}$ Å (Upper Right Section of Matrix) for Pairwise Structure Comparison[a]

	STZ2ap	STZ2a5mp	STZ2a5Clp	STZ2a5Brp
STZ2ap	x	20	18	29
STZ2a5mp	3.5	x	3	12
STZ2a5Clp	3.5	1.4	x	12
STZ2a5Brp	5.4	2.7	2.1	x

[a]Lower x and d values (in yellow) indicate better matching.

N1A−H1A···N1 among the structures. Strong intermolecular interactions are also observed between the amino group of STZ and oxygen atoms from the sulfo group. The N4−H41···O2 $(1/2 + x, 1/2 - y, -1/2 + z)$ hydrogen bond shows an intermediate character between closed shell and shared shell in each material $(E(r)/\rho(r) < 0)$, while the N4−H42···O1 $(1 + x, y, z)$ hydrogen bond is a closed-shell interaction $(E(r)/\rho(r) > 0)$. There are no meaningful differences in these contacts between STZ2a5Clp and STZ2a5Brp; however, these two hydrogen bonds are the strongest in STZ2ap. A different behavior is observed for the N1A−H1A2···N4 $(-1 + x, y, z)$ hydrogen bond, which is the weakest for STZ2ap. In each of the materials two weak interactions of C−H···O type are also observed. The C5A−H5A···O2 $(-1 + x, y, -1 + z)$ hydrogen bond is similar among the crystal structures, while that of C6A−H6A···O1 $(-1/2 + x, 1/2 - y, -1/2 + z)$ type is different. The latter interaction is the strongest in STZ2a5mp and the weakest in STZ2ap, whereas meaningless dissimilarities occur between STZ2a5Clp and STZ2a5Brp. The halogen atoms in STZ2a5Clp and STZ2a5Brp participate in the C3−H3···Cl/Br $(1/2 - x, -1/2 + y, 1/2 - z)$ hydrogen bond and S11···Cl/Br $(1 + x, y, 1 + z)$ chalcogen···halogen interaction. Each of these contacts have similar strengths in both crystal structures, although differences in contact distances are observed due to dissimilarities in the size of the halogen atom.

To quantify the similarities between the studied crystal structures, Hirschfeld surfaces and the fingerprint plots were studied.[57,58] The fingerprint plots for crystal components (Figures S5 and S6) show common features, proving that analogous intermolecular interactions are present in all of the materials. A detailed analysis of the percent contribution of intermolecular contacts shows similar values for the pair STZ2ap and STZ2a5mp and also for the pair STZ2a5Clp and STZ2a5Brp (Figure 4). The differences in contributions to X···H interactions between STZ2ap, STZ2a5mp and STZ2a5Clp, STZ2a5Brp can be easily explained by the presence of a halogen atom in the latter crystal structures instead of the substituent containing H atoms.

3.4. Refractive Indices. The theoretical and experimental results show that all of the examined crystals are biaxial, with

Table 3. Topological Analysis of Selected Intermolecular Interactions[a]

	d	d_1	d_2	ρ(r)	$\nabla^2\rho(r)$	V(r)	E(r)/ρ(r)	E_{int}
N8-H8···N2A								
STZ2ap	1.692	0.533	1.159	0.056	0.11	-0.0408	-0.125	-12.80
STZ2a5mp	1.682	0.528	1.154	0.058	0.11	-0.0423	-0.121	-13.27
STZ2a5Clp	1.711	0.543	1.168	0.053	0.11	-0.0383	-0.098	-12.02
STZ2a5Brp	1.712	0.544	1.168	0.054	0.11	-0.0383	-0.096	-12.02
N1A-H1A···N1								
STZ2ap	2.054	0.724	1.330	0.024	0.06	-0.0160	0.00	-5.02
STZ2a5mp	2.012	0.705	1.307	0.026	0.07	-0.0180	0.00	-5.65
STZ2a5Clp	2.044	0.719	1.325	0.024	0.06	-0.0164	-0.004	-5.15
STZ2a5Brp	2.052	0.723	1.329	0.024	0.06	-0.0162	-0.004	-5.08
N4-H41···O2[1/2+x,1/2-y,-1/2+z]								
STZ2ap	1.929	0.69	1.239	0.027	0.08	-0.0212	-0.037	-6.65
STZ2a5mp	1.989	0.721	1.268	0.024	0.07	-0.0186	-0.042	-5.84
STZ2a5Clp	1.962	0.709	1.253	0.025	0.07	-0.0198	-0.032	-6.21
STZ2a5Brp	1.984	0.720	1.264	0.024	0.07	-0.0188	-0.029	-5.90
N4-H42···O1[1+x,y,z]								
STZ2ap	1.958	0.721	1.237	0.023	0.08	-0.0185	0.043	-5.80
STZ2a5mp	2.059	0.774	1.285	0.019	0.06	-0.0151	0.005	-4.74
STZ2a5Clp	1.990	0.737	1.253	0.022	0.07	-0.0175	0.00	-5.49
STZ2a5Brp	1.986	0.734	1.252	0.022	0.07	-0.0177	0.00	-5.55
N1A-H1A2···N4[-1+x,y,z]								
STZ2ap	2.444	0.935	1.509	0.012	0.04	-0.0077	0.025	-2.42
STZ2a5mp	2.329	0.879	1.45	0.015	0.04	-0.0100	0.00	-3.14
STZ2a5Clp	2.336	0.885	1.451	0.015	0.04	-0.0100	0.027	-3.14
STZ2a5Brp	2.332	0.886	1.446	0.015	0.04	-0.0102	0.033	-3.20
C6A-H6A···O1[-1/2+x,1/2-y,-1/2+z]								
STZ2ap	2.462	0.997	1.465	0.010	0.03	-0.0067	0.030	-2.10
STZ2a5mp	2.315	0.919	1.396	0.013	0.04	-0.0096	0.031	-3.01
STZ2a5Clp	2.399	0.966	1.433	0.011	0.04	-0.0076	0.064	-2.38
STZ2a5Brp	2.413	0.973	1.44	0.010	0.03	-0.0073	0.070	-2.29
C5A-H5A···O2[-1+x,y,-1+z]								
STZ2ap	2.419	0.978	1.441	0.010	0.03	-0.0069	0.100	-2.16
STZ2a5mp	2.451	1.001	1.45	0.009	0.03	-0.0061	0.111	-1.91
STZ2a5Clp	2.403	0.972	1.431	0.009	0.03	-0.0067	0.089	-2.10
STZ2a5Brp	2.455	1.001	1.454	0.008	0.03	-0.0058	0.112	-1.84
S11···Halogen[1+x,y,1+z]								
STZ2a5Clp	3.469	1.714	1.755	0.008	0.03	-0.0038	0.188	-1.19
STZ2a5Brp	3.543	1.697	1.846	0.008	0.03	-0.0041	0.175	-1.29
C3-H3···Halogen[1/2-x,-1/2+y,1/2-z]								
STZ2a5Clp	2.695	1.04	1.655	0.009	0.03	-0.0050	0.200	-1.57
STZ2a5Brp	2.852	1.09	1.762	0.009	0.03	-0.0046	0.200	-1.44

[a]Definitions: d, intermolecular distance (Å); d_1, d_2, distances between bond critical point and interacting atoms (Å); $\rho(r)$, charge density (a.u.); $\nabla^2\rho(r)$, Laplacian of electron density (a.u.); $V(r)$, $E(r)$, local potential and total energy density (a.u.); $E_{int} = 1/2V(r)$ (kcal/mol).[56]

differences in optical signs. The crystals of STZ2ap, STZ2a5mp, and STZ2a5Clp are optically negative, whereas the STZ2a5Brp crystals are found to be optically positive (Table 4). For the halogen-containing structures the optical indicatrix axis related to the largest refractive index n_γ coincides with the b crystallographic axis, whereas for STZ2ap and STZ2a5mp the n_β refractive index can be measured in the

https://dx.doi.org/10.1021/acs.cgd.0c00743
Cryst. Growth Des. 2020, 20, 6535−6544

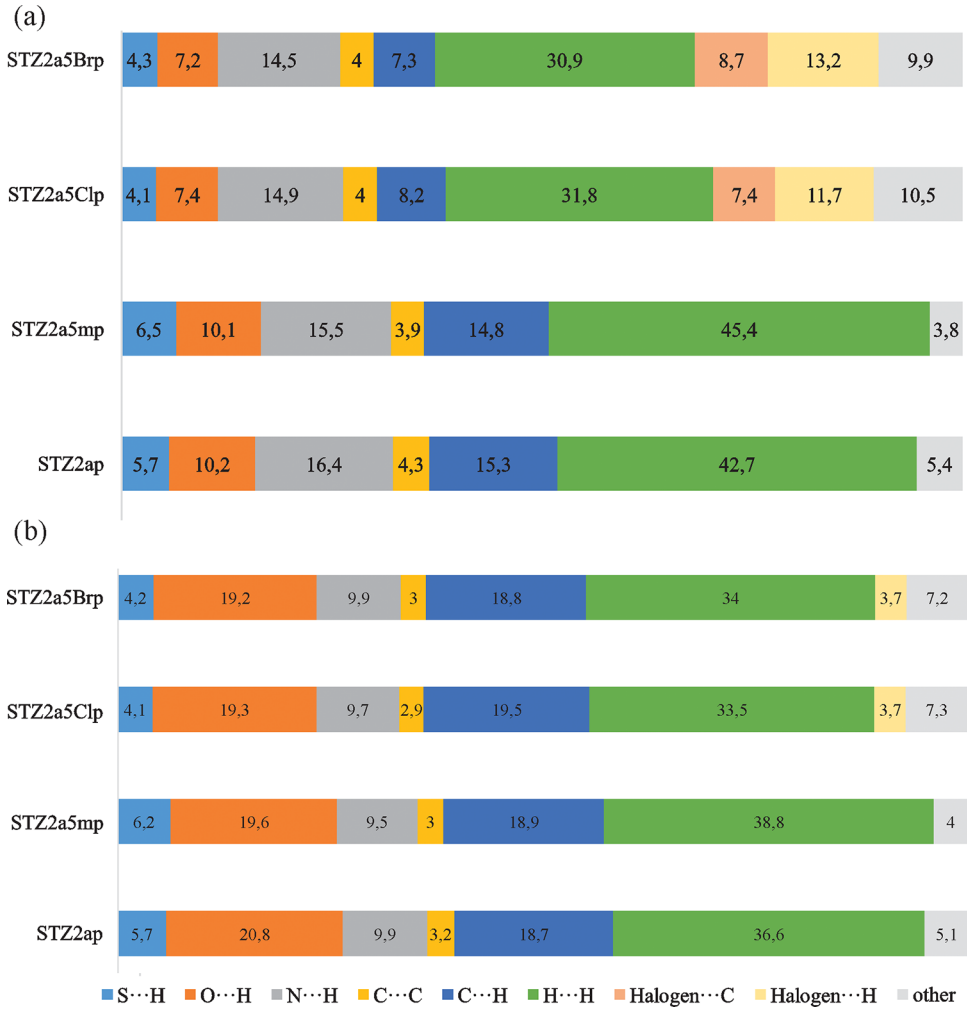

Figure 4. Percent contribution of weak interactions to Hirshfeld surface area for 2-aminopyridine and its derivatives (a) and the STZ molecule (b).

Table 4. Results of the Bulk Property Calculations at MP2 within the Q-LFT Level of Theory and Experimentally Measured Values[a]

	λ/nm	n_α	n_β	n_γ
STZ2ap	532	1.632	1.708	1.710
exptl		1.66	1.69	1.71
STZ2a5mpA	532	1.628	1.709	1.714
exptl		1.67	1.72	1.74
STZ2a5mpB	532	1.639	1.715	1.729
exptl		1.67	1.72	1.74
STZ2a5Clp	532	1.633	1.711	1.717
exptl		1.67	1.70	1.74
STZ2a5Brp	532	1.629	1.710	1.720
exptl		1.66	1.72	1.79

[a]Standard deviations for the experimental values are smaller than that of 0.01.

[010] direction (Figure 5). The remaining two refractive indices are located in the *ac* plane, and the two optical indicatrix axis directions, representing n_β or n_γ, always coincide with the direction of the strongest hydrogen bonds found in those structures (marked in magenta in Figure S2). However, there is no obvious correlation between the strength of the hydrogen bonds and the changes observed in the optical indicatrix. In the STZ2a5Clp and STZ2a5Brp structures (Figure S8 and Table3) one of the indicatrix main axes related to n_β is close to that of the strongest interactions (ca. −24.47/−24.76 kcal/mol, respectively), whereas the other axis associated with the largest n_γ can be correlated with only a minor intermolecular interaction strength (ca. −2.29/−2.38 kcal/mol). The opposite can be found for $-CH_3$ and −H substituted derivatives—the n_γ value was measured close to the direction of the strongest interactions (−25.57/−25.78 kcal/mol), and n_β coincides with only a weak hydrogen bond (ca. −3.01/−2.10 kcal/mol). Similarly, the fluctuations in hydrogen bond geometric parameters are negligible in comparison to the changes in the linear birefringence. The observed small variations in the orientation of optical indicatrix axes in the *ac* plane in the analyzed crystals can be attributed to the change in the character and size of pyridine substituents. Overall, the largest discrepancies between the refractive indices are observed between STZ2ap and STZ2a5Brp. This trend can be explained on the basis of a frequency-dependent molecular polarizability analysis (Table 5). As was expected, the polarizabilities show increasing values for substituted pyridines going from − H to $-CH_3$ and −Cl and finally the largest value can be found for −Br. On the other hand, the values obtained for the STZ molecule are almost identical across all structures. The exception is STZ2a5mp, where the increase in the STZ polarizability, as a result of salt formation, can be responsible for the largest refractive index observed in the *ac* plane. A

https://dx.doi.org/10.1021/acs.cgd.0c00743
Cryst. Growth Des. 2020, 20, 6535−6544

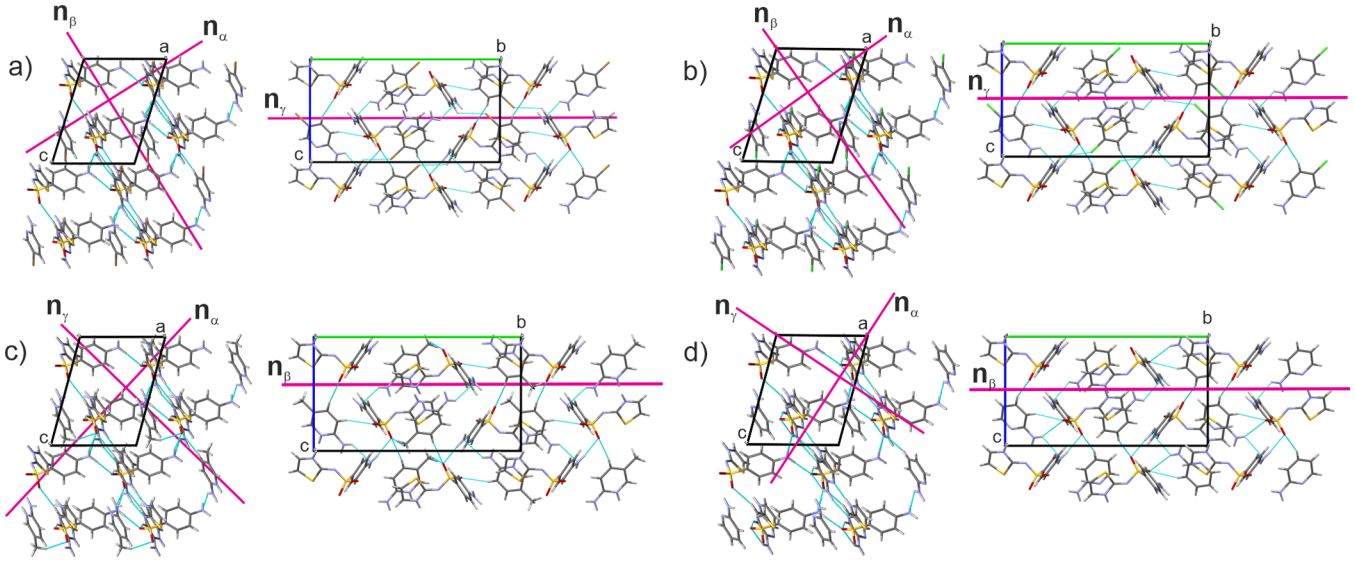

Figure 5. Experimentally determined orientation of indicatrix axes (magenta) with respect to the structural features of the materials: (a) STZ2a5Brp; (b) STZ2a5Clp; (c) STZ2a5mp; (d) STZ2ap.

Table 5. Frequency-Dependent Isotropic Molecular Polarizability (MP2)[a]

	2-aminopyridine derivative	STZ
STZ2ap	78.32	191.78
STZ2a5mpA	92.07	192.09
STZ2a5mpB	87.2	200.06
STZ2a5mp_av.	89.64	196.08
STZ2a5Clp	92.49	191.83
STZ2a5Brp	100.53	191.46

[a] λ = 532 nm. STZ2a5mp_av. is the average value of polarizability for structures A and B reflecting the situation in a crystal. Values are given in bohr^3.

similarity in refractive indices is observed for n_α, where both the values of refractive indices and the corresponding directions of optical indicatrix axes in the examined structures are almost identical. This can be explained by a simple analysis showing which directions in the crystals are the most and the least affected by the change in the substituent and at the same time molecular polarizability. The n_α value was found almost perpendicular to the pyridine ring planes, in close vicinity to the weak dispersive interactions between the pyridine and thiazole rings, and as such is the least affected by substitution. The electronic properties of the system change the most in the *b* direction—the closest to the direction of the dipole moment in substituted pyridines (Figure S9). On going from halogen to $-CH_3$ and $-H$ substituents, [010] is the direction of the optical indicatrix axis associated with the largest refractive index in STZ2a5Brp and STZ2a5Clp, whereas for STZ2a5mp and STZ2ap n_γ shifts to the *ac* plane as in those structures the impact of packing effects increases.

4. CONCLUSIONS

In this work, crystal structures and refractive indices of multicomponent materials containing sulfathiazole and 2-aminopyridine substituted in the *para* position by H/CH_3/Cl/Br were studied. The examined solids follow the symmetry of the $P2_1/n$ space group with similar unit cell parameters. The materials were found to be isostructural. In all of the crystal structures, a basic building unit formed by one sulfathiazole molecule and one 2-aminopyridine derivative molecule connected via two N−H···N type hydrogen bonds can be recognized. The basic building units are connected via N−H···O hydrogen bonds between STZ molecules, forming a layer expanding in the (010) plane. The layers repeat along [010] by inversion, and their relative orientation is stabilized by the presence of $\pi\cdots\pi$ and C−H···π interactions.

An analysis of the qualitative parameters describing isostructurality shows that the similarity of the geometrical arrangement of molecules in all of the crystal structures depends on the 2-aminopyridine substituent. As a methyl group and a chlorine atom are known to exhibit similar sizes and shapes, the interchange $CH_3 \rightarrow Cl$ does not significantly influence the crystal architecture. The smallest similarity of crystal packing is observed for H → Br exchange, which can be easily explained by their size difference. However, the resulting optical indicatrix of the crystalline materials has a similar structure−property relationship for Cl and Br derivatives that is different from those of H and CH_3, indicating the significance of the electronic properties and polarizability of the substituents. In all of the materials, the smallest refractive index n_α has nearly identical values and can be measured in approximately the same direction. The optical indicatrix axis associated with the largest refractive index for STZ2a5Clp and STZ2a5Brp is in the [100] direction, while in STZ2a5mp and STZ2ap it is in the (101) plane. It is worth mentioning that, despite large differences between the electronic properties of the substituents −H, $-CH_3$, −Cl and −Br, the observed variations in molecular polarizabilities cause rather small changes in the observed refractive indices. The maximum birefringences obtained remain almost identical for STZ2a5mp, STZ2a5Clp, and STZ2ap (in the range 0.05−0.07). For STZ2a5Brp we observe slightly the larger value 0.13, which is not as significant an increase as one might expect. This result is very important, as it shows the influence of crystal packing on the size of the linear optical properties. A significant increase in birefringence cannot be expected when only small changes to one component are introduced while the crystal structure retains almost identical crystal packing. Linear

https://dx.doi.org/10.1021/acs.cgd.0c00743
Cryst. Growth Des. 2020, 20, 6535−6544

optical properties are not solely dependent on the values of molecular polarizabilities but are strongly influenced by the relative arrangement of the crystal building blocks guided by intermolecular interactions. In the case of −H and $-CH_3$ the packing effects seem to dominate over the substituent effect as opposed to the −Cl and −Br cases, where the effect of the substituent determines the observed changes in the optical indicatrix. Hence, both the design of new compounds and crystal engineering procedures need to be employed simultaneously in order to obtain materials with programmed linear birefringence.

■ ASSOCIATED CONTENT

Supporting Information

The Supporting Information is available free of charge at https://pubs.acs.org/doi/10.1021/acs.cgd.0c00743.

Crystal data and structure refinement details, structural parameters (both experimental and calculated for optimized structures), results of refractive index measurements, asymmetric units with atom-numbering schemes, details on hydrogen bonding and weak dispersive interactions, results of isostructurality analysis using CrystalCMP software and packing similarity tool from the Mercury program, fingerprint plots, dispersion of refractive indices, and dipole moments of the molecules (PDF)

Accession Codes

CCDC 2004925−2004928 contain the supplementary crystallographic data for this paper. These data can be obtained free of charge via www.ccdc.cam.ac.uk/data_request/cif, or by emailing data_request@ccdc.cam.ac.uk, or by contacting The Cambridge Crystallographic Data Centre, 12 Union Road, Cambridge CB2 1EZ, UK; fax: +44 1223 336033.

■ AUTHOR INFORMATION

Corresponding Author

Marlena Gryl − *Faculty of Chemistry, Jagiellonian University, 30-387 Kraków, Poland;* orcid.org/0000-0003-2267-1588; Email: gryl@chemia.uj.edu.pl

Authors

Joanna Wojnarska − *Faculty of Chemistry, Jagiellonian University, 30-387 Kraków, Poland*

Tomasz Seidler − *Faculty of Chemistry, Jagiellonian University, 30-387 Kraków, Poland*

Katarzyna M. Stadnicka − *Faculty of Chemistry, Jagiellonian University, 30-387 Kraków, Poland;* orcid.org/0000-0002-3898-5824

Complete contact information is available at: https://pubs.acs.org/10.1021/acs.cgd.0c00743

Author Contributions

The manuscript was written through contributions of all authors. All authors have given approval to the final version of the manuscript.

Funding

Funding for this research was provided by the National Science Centre of Poland, grant No. 2018/29/N/ST5/00634 and grant No. 2018/30/E/ST5/00638.

Notes

The authors declare no competing financial interest.

■ ACKNOWLEDGMENTS

The authors acknowledge that parts of this work were supported by the PL-Grid Infrastructure. X-ray diffraction experiments were carried out using equipment purchased thanks to the financial support of the European Regional Development Fund in the framework of the Polish Innovation Economy Operational Program (contract no. POIG.02.01.00-12-023/08)

■ REFERENCES

(1) Desiraju, G. R. Supramolecular Synthons in Crystal Engineering-A New Organic Synthesis. *Angew. Chem., Int. Ed. Engl.* **1995**, *34*, 2311−2327.

(2) Shaikh, S. R.; Gawade, R. L.; Kumar, D.; Kotmale, A.; Gonnade, R. G.; Stűrzer, T. Crystal Engineering for Intramolecular $\pi-\pi$ Stacking: Effect of Sequential Substitution of F on Molecular Geometry in Conformationally Flexible Sulfonamides. *Cryst. Growth Des.* **2019**, *19*, 5665−5678.

(3) Yao, Z.-F.; Wang, J.-Y.; Pei, J. Control of $\pi-\pi$ Stacking via Crystal Engineering in Organic Conjugated Small Molecule Crystals. *Cryst. Growth Des.* **2018**, *18*, 7−15.

(4) Joseph, L.; Sajan, D.; Shettigar, V.; Chaitanya, K.; Misra, N.; Sundius, T.; Němec, I. Synthesis, Crystal Growth, Thermal Studies and Scaled Quantum Chemical Studies of Structural and Vibrational Spectra of the Highly Efficient Organic NLO Crystal: 1-(4-Aminophenyl)-3-(3,4-Dimethoxyphenyl)-Prop-2-En-1-One. *Mater. Chem. Phys.* **2013**, *141*, 248−262.

(5) Danel, A.; Wojtasik, K.; Szlachcic, P.; Gryl, M.; Stadnicka, K. A New Regiospecific Synthesis Method of 1H-Pyrazolo[3,4-b]-Quinoxalines − Potential Materials for Organic Optoelectronic Devices, and a Revision of an Old Scheme. *Tetrahedron* **2017**, *73*, 5072−5081.

(6) Ostrowska, K.; Musielak, B.; Szneler, E.; Dudek, Ł.; Gryl, M.; Stadnicka, K. Chelate Ring Size Effect as a Factor of Selective Fluorescent Recognition of Zn2+ Ions by Pyrrolo[2,3-b]Quinoxaline with a Substituted 2-Pyridyl Group Receptor. *Inorg. Chem.* **2015**, *54*, 8423−8435.

(7) Goud, N. R.; Zhang, X.; Brédas, J. L.; Coropceanu, V.; Matzger, A. J. Discovery of Non-Linear Optical Materials by Function-Based Screening of Multi-Component Solids. *Chem.* **2018**, *4*, 150−161.

(8) Gryl, M.; Stadnicka, K. Rubidium 2,4,6-Trioxo-1,3-Diazinan-5-Ide-1,3-Diazinane-2,4,6-Trione-Water (1/1/1). *Acta Crystallogr., Sect. E: Struct. Rep. Online* **2011**, *E67*, m571−m572.

(9) Gryl, M.; Cenedese, S.; Stadnicka, K. Crystal Engineering and Charge Density Study of Pharmaceutical Nonlinear Optical Material: Melamine-Barbital Co-Crystal. *J. Phys. Chem. C* **2015**, *119*, 590−598.

(10) Wang, K.; Zhang, H.; Chen, S.; Yang, G.; Zhang, J.; Tian, W.; Su, Z.; Wang, Y. Organic Polymorphs: One-Compound-Based Crystals with Molecular-Conformation- and Packing-Dependent Luminescent Properties. *Adv. Mater.* **2014**, *26*, 6168−6173.

(11) Upadhyay, P.; Khomane, K. S.; Kumar, L.; Bansal, A. K. Relationship between crystal structure and mechanical properties of ranitidine hydrochloride polymorphs. *CrystEngComm* **2013**, *15*, 3959−3964.

(12) Cinčić, D.; Friščić, T.; Jones, W. A cocrystallisation-based strategy to construct isostructural solids. *New J. Chem.* **2008**, *32*, 1776−1781.

(13) Fábián, L.; Kálmán, A. Volumetric measure of isostructurality. *Acta Crystallogr., Sect. B: Struct. Sci.* **1999**, *55*, 1099−1108.

(14) Dwichandra Putra, O.; Yonemochi, E.; Uekusa, H. Isostructural Multicomponent Gliclazide Crystals with Improved Solubility. *Cryst. Growth Des.* **2016**, *16*, 6568−6573.

(15) Suresh, K.; Rao Khandavilli, U. B.; Gunnama, A.; Nangia, A. Polymorphism, isostructurality and physicochemical properties of glibenclamide salts. *CrystEngComm* **2017**, *19*, 918−929.

(16) Dey, A.; Desiraju, G. R. Supramolecular equivalence of ethynyl, chloro, bromo and iodo groups. A comparison of the crystal structures of some 4-phenoxyanilines. *CrystEngComm* **2004**, *6*, 642−646.

(17) Landenberger, K. B.; Bolton, O.; Matzger, A. J. Two Isostructural Explosive Cocrystals with Significantly Different Thermodynamic Stabilities. *Angew. Chem., Int. Ed.* **2013**, *52*, 6468−6471.
(18) An, G.; Li, S.; Yan, X.; Yuan, Z.; Zhang, X. High-birefringence photonic crystal fiber polarization filter based on surface plasmon resonance. *Appl. Opt.* **2016**, *55*, 1262−1266.
(19) Chen, K.; Yang, Y.; Peng, G.; Yang, S.; Yan, T.; Fan, H.; Lin, Z.; Ye, N. A2Bi2(SO4)2Cl4 (A = NH4, K, Rb): achieving a subtle balance of the large second harmonic generation effect and sufficient birefringence in sulfate nonlinear optical materials. *J. Mater. Chem. C* **2019**, *7*, 9900−9907.
(20) Sylvester-Hvid, K. O.; Åstrand, P.-O.; Ratner, M. A.; Mikkelsen, K. V. Frequency-Dependent Molecular Polarizability and Refractive Index: Are Substituent Contributions Additive? *J. Phys. Chem. A* **1999**, *103*, 1818−1821.
(21) Lorentz, H. A. *The Theory of Electrons*; Dover: New York, 1952.
(22) Böttcher, C. J. F. *Theory of Electric Polarization*, 2nd ed.; Elsevier: Amsterdam, 1973; Vol. *1*.
(23) Dos Santos, L. H. R.; Macchi, P. The Role of Hydrogen Bond in Designing Molecular Optical Materials. *Crystals* **2016**, *6*, 43.
(24) Gryl, M.; Seidler, T.; Wojnarska, J.; Stadnicka, K. M.; Matulková, I.; Němec, I.; Němec, P. Co-Crystals of 2-Amino-5-Nitropyridine Barbital with Extreme Birefringence and Large Second Harmonic Generation Effect. *Chem. - Eur. J.* **2018**, *24*, 8727−873.
(25) Wojnarska, J.; Gryl, M.; Seidler, T.; Stadnicka, K. M. Crystal Engineering, Optical Properties and Electron Density Distribution of Polar Multicomponent Materials Containing Sulfanilamide. *CrystEngComm* **2018**, *20*, 3638−3646.
(26) Wojnarska, J.; Gryl, M.; Seidler, T.; Rydz, A.; Oszajca, M.; Stadnicka, K. M.; Marzec, M.; Matulková, I.; Němec, I.; Němec, P. Crystal Structure and (Non)Linear Optical Properties of a Cyanuric Acid Isoniazid < 1/1> Co-Crystal: Shortcomings of Phase Matching Determination from Powdered Samples. *Cryst. Growth Des.* **2019**, *19*, 6831−6836.
(27) Sarma, J. A. R. P.; Desiraju, G. R. The Role of Cl···Cl and C-H···O Interactions in the Crystal Engineering of 4-Å Short-Axis Structures. *Acc. Chem. Res.* **1986**, *19*, 222−228.
(28) Giangreco, I.; Cole, J. C.; Thomas, E. Mining the Cambridge Structural Database for Matched Molecular Crystal Structures: A Systematic Exploration of Isostructurality. *Cryst. Growth Des.* **2017**, *17*, 3192−3203.
(29) Stein, P. D.; Hunt, J. T.; Floyd, D. M.; Moreland, S.; Dickinson, K. E. J.; Mitchell, C.; Liu, E. C.-K.; Webb, M. L.; Murugesan, N.; Dickey, J.; McMullen, D.; Zhang, R.; Lee, V. G.; Serafino, R.; Delaney, C.; Schaeffer, T. R.; Kozlowski, M. The Discovery of Sulfonamide Endothelin Antagonists and the Development of the Orally Active ET_A Antagonist 5-(Dimethylamino)-N-(3,4-dimethyl-5-isoxazolyl)-l-naphthalenesulfonamide. *J. Med. Chem.* **1994**, *37*, 329−331.
(30) Gelbrich, T.; Hughes, D. S.; Hursthouse, M. B.; Threlfall, T. L. Packing similarity in polymorphs of sulfathiazole. *CrystEngComm* **2008**, *10*, 1328−1334.
(31) Thakuria, R.; Nath, N. K.; Roy, S.; Nangia, A. Polymorphism and Isostructurality in Sulfonylhydrazones. *CrystEngComm* **2014**, *16*, 4681.
(32) Gelbrich, T.; Threlfall, T. L.; Hursthouse, M. B. XPac dissimilarity parameters as quantitative descriptors of isostructurality: the case of fourteen 4,5′-substituted benzenesulfonamido-2-pyridines obtained by substituent interchange involving CF_3/I/Br/Cl/F/Me/H. *CrystEngComm* **2012**, *14*, 5454−5464.
(33) Gelbrich, T.; Hursthouse, M. B.; Threlfall, T. L. Structural systematics of 4,4′-disubstituted benzenesulfonamidobenzenes.1. Overview and dimer based isostructures. *Acta Crystallogr., Sect. B: Struct. Sci.* **2007**, *63*, 621−632.
(34) Gelbrich, T.; Hursthouse, M. B. A versatile procedure for the identification, description and quantification of structural similarity in molecular crystals. *CrystEngComm* **2005**, *7*, 324−336.
(35) Rohlíček, J.; Skořepová, E.; Baborb, M.; Čejka, J. CrystalCMP: an easy-to-use tool for fast comparisonof molecular packing. *J. Appl. Crystallogr.* **2016**, *49*, 2172−2183.
(36) Macrae, C. F.; Bruno, I. J.; Chisholm, J. A.; Edgington, P. R.; McCabe, P.; Pidcock, E.; Rodriguez-Monge, L.; Taylor, R.; van de Streek, J.; Wood, P. A. Mercury CSD 2.0 − new features for the visualization and investigation of crystal structures. *J. Appl. Crystallogr.* **2008**, *41*, 466−470.
(37) Seidler, T.; Stadnicka, K.; Champagne, B. Investigation of the linear and second-order nonlinear optical properties of molecular crystals within the local field theory. *J. Chem. Phys.* **2013**, *139*, 114105.
(38) Seidler, T.; Stadnicka, K.; Champagne, B. Linear and second-order nonlinear optical properties of ionic organic crystals. *J. Chem. Phys.* **2014**, *141*, 104109.
(39) Seidler, T.; Stadnicka, K.; Champagne, B. Erratum: Linear and second-order nonlinear optical properties of ionic organic crystals [J. Chem. Phys. 141, 104109 (2014)]. *J. Chem. Phys.* **2015**, *142*, 239901.
(40) Seidler, T.; Krawczuk, A.; Champagne, B.; Stadnicka, K. QTAIM-based scheme for describing the linear and nonlinear optical susceptibilities of molecular crystals composed of molecules with complex shapes. *J. Phys. Chem. C* **2016**, *120*, 4481−4494.
(41) Gryl, M.; Kozieł, M.; Stadnicka, K. M. A proposal for coherent nomenclature of multicomponent crystals. *Acta Crystallogr., Sect. B: Struct. Sci., Cryst. Eng. Mater.* **2019**, *75*, 53−58.
(42) *CrysAlisPro 171.38.41r* (2015) and *CrysAlisPro 1.171.40.14e* (2018); Rigaku Oxford Diffraction: Yarnton, England.
(43) Sheldrick, G. M. SHELXT − Integrated space-group and crystal structure determination. *Acta Crystallogr., Sect. A: Found. Adv.* **2015**, *71*, 3−8.
(44) Altomare, A.; Cascarano, G.; Giacovazzo, C.; Guagliardi, A.; Burla, M. C.; Polidori, G.; Camalli, M. SIR92 − a program for automatic solution of crystal structures by direct methods. *J. Appl. Crystallogr.* **1994**, *27*, 435.
(45) Sheldrick, G. M. Crystal structure refinement with SHELXL. *Acta Crystallogr., Sect. C: Struct. Chem.* **2015**, *71*, 3−8.
(46) Dovesi, R.; Erba, A.; Orlando, R.; Zicovich-Wilson, C. M.; Civalleri, B.; Maschio, L.; Rérat, M.; Casassa, S.; Baima, J.; Salustro, S.; Kirtman, B. Quantum-mechanical condensed matter simulations with CRYSTAL. *WIREs Comput. Mol. Sci.* **2018**, *8*, e1360.
(47) Dovesi, R.; Saunders, V. R.; Roetti, C.; Orlando, R.; Zicovich-Wilson, C. M.; Pascale, F.; Civalleri, B.; Doll, K.; Harrison, N. M.; Bush, I. J.; D'Arco, P.; Llunell, M.; Causà, M.; Noël, Y.; Maschio, L.; Erba, A.; Rérat, M.; Casassa, S. *CRYSTAL17 User's Manual*; University of Torino: Torino, 2017.
(48) Gatti, C.; Saunders, V. R.; Roetti, C. Crystal field effects on the topological properties of the electron density in molecular crystals. The case of urea. *J. Chem. Phys.* **1994**, *101*, 10686−10696.
(49) Gatti, C.; Casassa, S. *TOPOND14 User's Manual*; CNR-ISTM of Milano: Milano, 2013.
(50) Frisch, M. J.; Trucks, G. W.; Schlegel, H. B.; Scuseria, G. E.; Robb, M. A.; Cheeseman, J. R.; Scalmani, G.; Barone, V.; Petersson, G. A.; Nakatsuji, H.; Li, X.; Caricato, M.; Marenich, A. V.; Bloino, J.; Janesko, B. G.; Gomperts, R.; Mennucci, B.; Hratchian, H. P.; Ortiz, J. V.; Izmaylov, A. F.; Sonnenberg, J. L.; Williams-Young, D.; Ding, F.; Lipparini, F.; Egidi, F.; Goings, J.; Peng, B.; Petrone, A.; Henderson, T.; Ranasinghe, D.; Zakrzewski, V. G.; Gao, J.; Rega, N.; Zheng, G.; Liang, W.; Hada, M.; Ehara, M.; Toyota, K.; Fukuda, R.; Hasegawa, J.; Ishida, M.; Nakajima, T.; Honda, Y.; Kitao, O.; Nakai, H.; Vreven, T.; Throssell, K.; Montgomery, J. A., Jr.; Peralta, J. E.; Ogliaro, F.; Bearpark, M. J.; Heyd, J. J.; Brothers, E. N.; Kudin, K. N.; Staroverov, V. N.; Keith, T. A.; Kobayashi, R.; Normand, J.; Raghavachari, K.; Rendell, A. P.; Burant, J. C.; Iyengar, S. S.; Tomasi, J.; Cossi, M.; Millam, J. M.; Klene, M.; Adamo, C.; Cammi, R.; Ochterski, J. W.; Martin, R. L.; Morokuma, K.; Farkas, O.; Foresman, J. B.; Fox, D. J. *Gaussian 16, Rev. C.01*; Gaussian, Inc.: Wallingford, CT, 2016.
(51) Keith, T. A. *AIMAll (Version 19.10.12)*; TK Gristmill Software: Overland Park, KS, USA, 2019 (aim.tkgristmill.com).

https://dx.doi.org/10.1021/acs.cgd.0c00743
Cryst. Growth Des. 2020, 20, 6535−6544

(52) Childs, S. L.; Stahly, G. P.; Park, A. The Salt-Cocrystal Continuum: The Influence of Crystal Structure on Ionization State. *Mol. Pharmaceutics* **2007**, *4*, 323−338.
(53) Johnson, E. R.; Keinan, S.; Mori-Sánchez, P.; Contreras-García, J.; Cohen, A. J.; Yang, W. Revealing Noncovalent Interactions. *J. Am. Chem. Soc.* **2010**, *132*, 6498−6506.
(54) Kálmán, A.; Párkányi, L.; Argay, G. Classification of the isostructurality of organic molecules in the crystalline state. *Acta Crystallogr., Sect. B: Struct. Sci.* **1993**, *49*, 1039−1049.
(55) Kálmán, A.; Argay, G.; Scharfenberg-Pfeiffer, D.; Hhne, E.; Ribár, N. 'Main-part' isostructuralism of several cardenolides and bufadienolides. Structures of three cardenolides: (21S)-methyldigitoxigenin, uzarigenin and sarmentogenin methanol solvate. *Acta Crystallogr., Sect. B: Struct. Sci.* **1991**, *47*, 68−77.
(56) Espinosa, E.; Alkorta, I.; Elguero, J.; Molins, E. From Weak to Strong Interactions: A Comprehensive Analysis of the Topological and Energetic Properties of the Electron Density Distribution Involving X−H···F−Y Systems. *J. Chem. Phys.* **2002**, *117*, 5529.
(57) Spackman, M. A.; Jayatilaka, D. Hirshfeld surface analysis. *CrystEngComm* **2009**, *11*, 19−32.
(58) Spackman, M. A.; McKinnon, J. J. Fingerprinting intermolecular interactions in molecular crystals. *CrystEngComm* **2002**, *4*, 378−392.

https://dx.doi.org/10.1021/acs.cgd.0c00743
Cryst. Growth Des. 2020, 20, 6535−6544